Sliding Mode Control Strategy for DC Microgrid Powered by Wind Energy, Diesel Generator and Energy Storage System with Pulsating Loads

www.rericjournal.ait.ac.th

Akhand Pratap Singh*, [1] Adeeb Uddin Ahmad*, and Kuldeep Sahay*

Abstract – This paper examines the use of sliding mode control (SMC) to enhance the operation of a DC Microgrid that includes wind energy, a diesel generator, and battery backup. The integration of renewable sources like wind introduces instability due to their intermittent nature. To address this, the Microgrid incorporates a diesel generator and battery backup to improve reliability and resilience during periods of low renewable energy. SMC is proposed as an effective control strategy for managing these challenges, offering benefits such as disturbance rejection and quick response. Through detailed simulations, the study demonstrates that SMC significantly improves the stability and performance of the Microgrid under various conditions. This approach highlights the potential of SMC to create more efficient and sustainable energy management systems in Microgrids with diverse energy sources.

1. INTRODUCTION

The integration of RES into microgrid systems has drawn a lot of attention lately because of the increased demand for robust and sustainable energy solutions. DC microgrid offer a promising platform for integrating varied energy sources, such as PV system, wind energy systems etc. while ensuring efficient power distribution and management. However, the intermittent nature of RES poses difficulties to the stable and reliable operation of Microgrid, requiring the incorporation of supplementary energy sources like diesel generators and battery backups. Conventional control strategies for microgrid often struggle to effectively manage the dynamic and uncertain nature of renewable energy generation, leading to suboptimal performance and reduced system stability. In this context, sophisticated control techniques, like sliding mode control (SMC), have emerged as promising solutions for addressing these challenges. SMC offers robustness against uncertainties and disturbances, making it well-suited for regulating the operation of microgrid with intermittent renewable energy sources.

Several studies have investigated the application of sliding mode control in various power system scenarios, demonstrating its effectiveness in achieving desired control objectives. For instance, proposing a SMC strategy for wind energy generation systems with PMSG (permanent magnet synchronous generators), highlighting its capacity to enhance system stability and execution [1]. Advanced control architectures for intelligent Microgrid, emphasizing the role of control strategies in improving power quality and energy storage management [2].

Despite these advancements, there remains a need for further research to explore the execution of SM control specifically in DC microgrid systems with multiple energy sources, including wind, diesel, and battery storage.

This paper seeks to close this gap by looking into the use of sliding mode control in optimizing the operation of a DC microgrid incorporating a diesel generator system, wind energy system and battery backup. The effectiveness of the suggested sliding mode control strategy will be assessed via in-depth simulation studies and experimental validation, with an emphasis on improving system stability, efficiency, and reliability.

By leveraging the advantages of sliding mode control and integrating it into DC microgrid systems, this study aids in the advancement of more robust and resilient energy management solutions capable of accommodating diverse renewable energy sources.

In this research gap is available as the wind energy module is used to serve the system load and the generator is used in combination. The controller robustness makes the controller more accurate for the DC microgrid the behavior pattern is studied in this paper with wind and the diesel generator.

2. DC MICROGRID MODELLING AND CONFIGURATION

2.1 DC Microgrid Configuration

DC microgrid systems are structured configurations designed to efficiently distribute and manage power within a localized area. These systems are composed of various components interconnected through a DC bus, facilitating streamlined power transfer and enhanced controllability [3]. Key elements of a typical DC microgrid include loads, power sources, and energy storage systems. The power sources in a DC microgrid often comprise renewable energy generators like photovoltaic (PV) arrays, fuel cells, and wind turbines, along with conventional sources such as batteries or

---
*EED, Institute of Engineering and Technology, Lucknow, U.P, India.

1
  Corresponding author;
Tel: +91 8318726804.
E-mail: 2200521685001@ietlucknow.ac.in.

diesel generators [4]. The PV array, for instance, converts solar energy into electrical power, while the fuel cell system utilizes chemical reactions to generate electricity [5]. Wind energy is transformed into mechanical power by the wind turbine, and converters convert this power to electrical power.

Figure 1 shows a overall schematic construction of the DC microgrid, which includes:

a. DC sources: These comprise diesel generators with the appropriate converter and wind turbines.
b. DC storage units: These comprise BESs and supercapacitors that have converters added.
c. Empties among these are DC-compatible loads. Through charge and discharge, the BES serves as the primary component for voltage regulation of a DC microgrid, maintaining power balance of system [6].
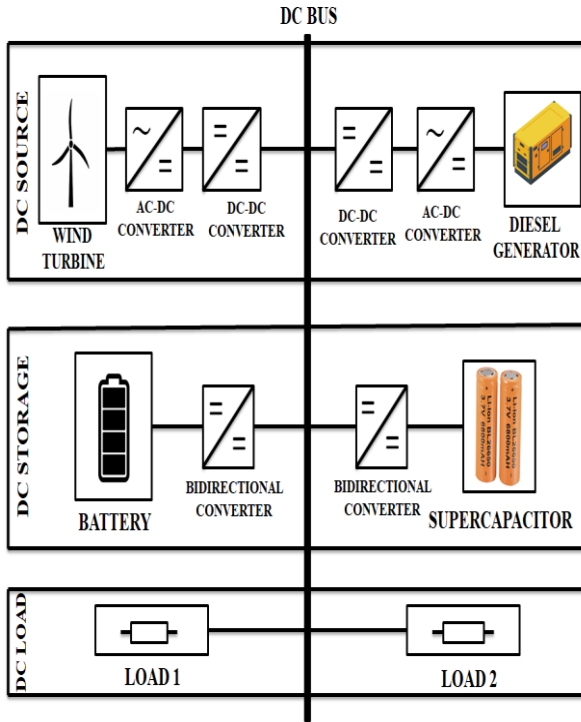

Fig. 1. Configuration of DC microgrid.

In a DC microgrid, excess electricity causes a surge in bus voltage and vice versa [7]. As a result, the controller keeps the DC microgrids power balance stable by discharging the BES when there is deficit power and charging it when there is extra power. The equation that follows can be used to express power balance on a DC microgrid:

$$P_{Energy\ Storage} = P_{Source} - P_{Load} \qquad (1)$$

Where, $P_{Energy\ Storage}$, P_{Source} and P_{Load} are the power of loads, DC sources, and battery energy storage devices, in that order.

2.2 Modeling of DC MG Components

2.2.1 Modeling of wind energy conversion system

Figure 2 depicts the wind power generation module model. It is a system that uses a generator to produce

electrical energy and transform wind energy into mechanical energy. The electrical DC grid side and the generator side make up the two main sections of this system. The generator side control is the main topic of this work.
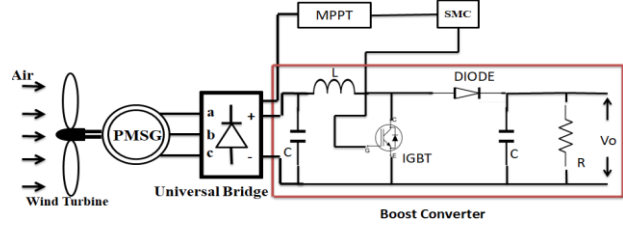

Fig. 2. Wind turbine with PMSG.

2.2.2 Mathematical modeling of wind turbine

Equations (2) and (3) can be used to express the wind's kinetic energy and power,

$$E = \tfrac{1}{2}mv^2 = \tfrac{1}{2}(\rho A v t)v^2 = \tfrac{1}{2}\rho A v^3 t \qquad (2)$$

$$P_w = \frac{E}{t} = \tfrac{1}{2}\rho A v^3 = \tfrac{1}{2}\rho\left(\pi R_b{}^2\right)v^3 = \tfrac{1}{2}\rho\pi R_b{}^2 v^3 \qquad (3)$$

Where P_w is the wind's potentially useful power, R_b is the wind power turbine's radius, A is the area the wind travels over, v is the wind's velocity, and t is the time. E is also the wind's kinetic energy. The wind's power as indicated in Equation (3) only represents the wind's maximum potential power. Actually, only a portion of this potential power can be generated by the wind turbine into electrical energy. The C_p (power coefficient) is the ratio of the power produced by the module of wind to the mechanical power that the turbine can produce. The output coefficient has a maximum value of 59.26%, often known as Betz's limit. However, its real value falls between around 25 and 45%, as shown in the following expressions [8, 9].

$$C_p = \frac{P_m}{P_w} \qquad (4)$$

$$C_p(\lambda,\beta) = c_1\left(c_2\frac{1}{\lambda_i} - c_3\beta - c_4\right)e^{-\frac{c_5}{\lambda_i}},$$
$$\frac{1}{\lambda_i} = \frac{1}{\lambda + 0.08\beta} - \frac{0.035}{\beta^3 + 1} \qquad (5)$$

In this case, β is the blade pitch angle, λ is the tip speed ratio, c_1=0.5, c_2=116, c_3=0.4, c_4=5, and c_5=21. The mechanical energy that can be recovered from the wind for wind power turbines can be expressed using Equations (3) and (4), as shown below:

$$P_m = \tfrac{1}{2}\rho\pi R_b{}^2 C_p(\lambda,\beta)v^3 \qquad (6)$$

Figure 3 depicts the power output for each wind speed based on how quickly the rotor rotates.
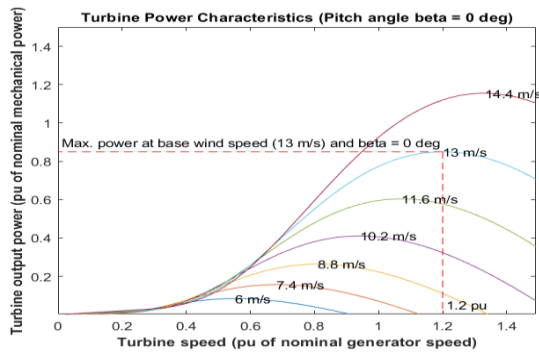
Fig. 3. Turbine speed v/s output power.

As may be observed, Figure 3 shows how wind speed affects the maximum output energy. The generator rotational speed at its highest output energy is known as the optimal rotor speed ($w_{opt} = w_{ref}$). MPPT (highest power point tracking) is a technique used to maintain this speed at each wind speed in order to acquire the maximum output energy [10, 11].

One of the key components in MPPT algorithms. Figure 4 is the voltage reference (v_{ref}). V_{ref} provides a stable reference voltage against which the voltage output of the wind module is contrasted, enabling the MPPT controller to adjust the operating point of the solar panels accordingly. Through constant monitoring of the maximum power point (MPP), of the wind module, MPPT controllers ensure the system functions as efficiently as possible, thereby maximizing the energy yield.

The fundamental idea behind MPPT with V_{ref} is to alter the wind module operating point and track the resulting shift in power output. To accomplish this optimization, a number of methods have been devised, including fractional open circuit voltage, perturb and observe (P&O) and incremental conductance. To set the reference voltage for comparison and decision-making, these algorithms rely on V_{ref} [12].
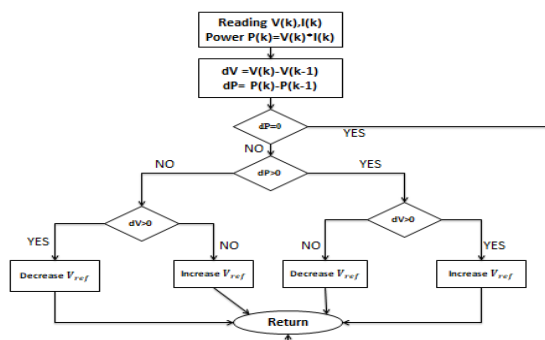

Fig. 4. MPPT algorithm.

2.2.3 Modeling of diesel generator (DG)

Like a lot of electromechanical systems that generate electricity, a DG may be broken down into three fundamental components (Figure 4a): the automated voltage regulator (AVR), the prime mover (PM) and the synchronous generator (SG), which is made up of an engine and a speed governor (Figure 4b). A steady speed operation is guaranteed by the speed governor, while the AVR maintains the generated voltage under various load conditions.
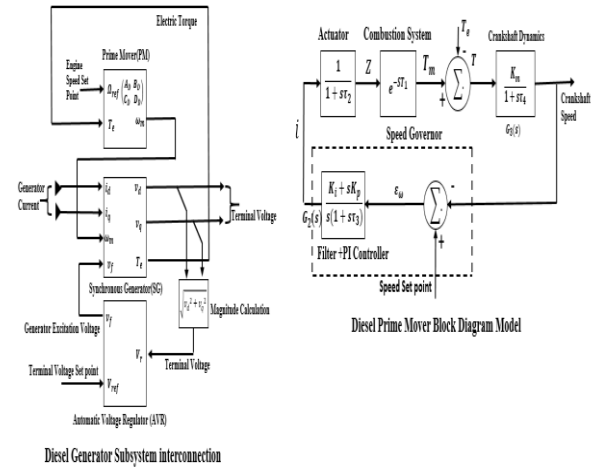

Fig. 4a. Diesel generator interconnection, 4b. diesel prime mover block

2.2.4 Prime mover modeling

A simplified representation of the prime mover structure is provided in Figure4b. First-order transfer functions that are basic and have temporal constants τ_1, τ_4, and τ_3 are used to simulate speed sensing, crankshaft dynamics, and the fueling actuator in that order, respectively. With the integrator and proportional gains k_p and k_i, respectively, the governors, it is described as a straightforward PI controller [13] – [16]. As the current study focuses on the formulation of the diesel generator's state model, the TF G1(s), G2(s), and G3(s) shown in Figure 2 are arranged in a compact space form.

$$pX_D = A_D X_D + B_D U_D$$
$$Y_D = C_D X_D \tag{7}$$

Where, $p = \dfrac{d(*)}{dt}$ the derivative operator is this. The linear system theory's observable canonical realization is used to obtain (7). The matrices and model vectors (state, input, and output) are provided by (8)–(10).

$$X_D = [x_1 \;\dots\; x_5]^T \;;\; U_D = [\Omega_{ref} \; T_e]^T \tag{8}$$

Every quantity is stated using the per unit approach. The state space variables x_1, x_3 and x_5 are respectively, three factors: crankshaft rotation speed, fuel rack position, and mechanical torque, while x_2 and x_4 are some intermediate state variables.

$$A_D = \begin{bmatrix} \frac{2\tau_2-\tau_1}{\tau_1\tau_2} & 1 & \frac{-1}{\tau_2} & 0 & 0 \\ \frac{-1}{\tau_1\tau_2} & 0 & \frac{1}{\tau_1\tau_2} & 0 & 0 \\ 0 & 0 & \frac{-1}{\tau_3} & 1 & \frac{K_p}{\tau_3} \\ 0 & 0 & 0 & 0 & \frac{K_i}{\tau_3} \\ \frac{K_m}{\tau_4} & 0 & 0 & 0 & \frac{-1}{\tau_4} \end{bmatrix} B_D = \begin{bmatrix} 0 & 0 \\ 0 & 0 \\ \frac{K_p}{\tau_3} & 0 \\ \frac{K_i}{\tau_3} & 0 \\ 0 & \frac{-K_m}{\tau_4} \end{bmatrix} \quad (9)$$

$$C_D = \begin{bmatrix} 0 & 0 & 0 & 0 & 1 \\ 1 & 0 & 0 & 0 & 0 \\ 0 & 0 & 1 & 0 & 0 \end{bmatrix}; \quad Y_D = [\omega_m \;\; T_m \;\; i]^T \quad (10)$$

2.2.5 Synchronous machine modeling

Large disturbance tests that synchronous generators are known to be safe to use, like load rejection and open armature circuit field short-circuit test, have been selected for this investigation [17]. As a result, this work provides an overview of the model of the SG known as the hybrid state, which was created in [17] and is ideally suited for estimating performance following the previously specified decrement tests. It is possible to express the SG flow and voltage equations in matrix forms (11)–(12).

• Flux equations:

$$\begin{bmatrix} \Psi_s \\ \Psi_r \end{bmatrix} = \begin{bmatrix} -X_s & X_{ST} \\ -X_{ST}{}^T & X_r \end{bmatrix} \begin{bmatrix} I_s \\ I_r \end{bmatrix} \quad (11)$$

• Voltage equations:

$$\begin{bmatrix} V_s \\ V_r \end{bmatrix} = \begin{bmatrix} R_s & O_{2,3} \\ O_{3,2} & R_r \end{bmatrix} \begin{bmatrix} I_s \\ I_r \end{bmatrix} + \left(\frac{pI_5}{\omega_n} + \begin{bmatrix} \omega_m & O_{2,3} \\ O_{3,2} & O_{3,3} \end{bmatrix} \right) \begin{bmatrix} \Psi_s \\ \Psi_r \end{bmatrix} \quad (12)$$

Where:

$$\Psi_s = [\psi_d \;\; \psi_q]^T \; ; \;\; \Psi_r = [\psi_f \;\; \psi_D \;\; \psi_Q]^T \quad (13)$$

$$V_s = [v_d \;\; v_q]^T \; ; \;\; V_r = [v_f \;\; 0 \;\; 0]^T \quad (14)$$

$$I_s = [i_d \;\; i_q]^T \; ; \;\; I_r = [i_f \;\; i_D \;\; i_Q]^T \quad (15)$$

Using (11)–(12) and the technique established in [17], the so-called synchronous machine hybrid state model is stated in state space compact form (16):

$$\begin{aligned} pX_G &= A_G X_G + B_G U_G \\ Y_G &= C_G X_G + D_G U_G \end{aligned} \quad (16)$$

With,

$$\begin{aligned} Y_G &= [i_f \;\; v_d \;\; v_q]^T \; ; \;\; U_G = [v_f \;\; i_d \;\; i_q]^T; \\ X_G &= \Psi_r \end{aligned} \quad (17)$$

The primary matrices of this state model, AG, BG, CG, and DG, are provided in [17]. The reality that the state apparatus (7) is unbending is an intriguing observation. In actuality, the speed dynamic and the electrical torque in (7) are a straight line, as seen in [17] for the full load rejection test.

3. CONTROLLER METHODOLOGY FOR DIFFERENT SOURCES

3.1 SMC Methodology for Wind Energy

A design process that ensures null overshoot, the intended settling time, and system stability is required for the SMC to operate. Therefore, during this design phase, every part of the control feedback loops, including the requirements of the MPPT V_{ref} algorithm, SMCs, gains, etc. must be taken into account. Wind voltage behavior can also be explained by including the reference and derivative of voltage error in the switching function, or V_{wind}. The input capacitor's current $(i_{C_{in}})$ can be measured to determine the voltage derivative. The MATLAB/SIMULINK Model presented in Fig 6. The primary benefit of using such a switching function is that it allows for wind voltage regulation without the need for extra controllers that rely on linearized models. Therefore, the surface and switching function are given in Equation (18) form the basis of this work and enable the investigation of wind voltage stability when load, environment, and reference fluctuations are present.

$$\psi = (V_{wind} - V_{ref}).k_1 + i_{C_{in}}.k_2 \;\; \wedge \;\; \varphi = \{\Psi = 0\} \quad (18)$$

It is important to notice that this kind of switching function, Ψ, is similar to the equivalent switching function used in [18]. To ensure stable SMC behavior and accurate MPP tracking, this design, however, focuses on offering a novel analytical and draft approach for the controlling, eschewing all of the simplifications employed in [19]. It is noteworthy to mention that this type of switching function, is comparable to the one used in [20], which is an equivalent switching function. To ensure stable SMC behavior and accurate MPP tracking, this design, however, focuses on offering a revised procedure for control system analysis and design, excluding all of the simplifications employed in [20].

$$i_{C_{in}} = C_{in}.\frac{d_{VPV}}{dt} = i_{wind} - i_L \quad (19)$$

$$V_L = L.\frac{di_L}{dt} = V_{wind} - V_b.(1 - u) \quad (20)$$

Capacitor current modeling could be done using the untangled single diode model [19], [18]. The thermal voltage in this model is dependent on the wind temperature and is represented by the variables i_{sc} (short-circuit current) and i_r (diode saturation current) [20]. This model's parameters can be calculated using the numbers on the data sheet and the operating state, as mentioned in [19], where the irradiance and the short-circuit current are about proportionate, or $i_{sc} = k_s.S$.

$$i_{wind} = i_{SC} - I_R.(e^{\alpha.V_{wind}} - 1) \quad (21)$$

The wind turbine system model and the SMC structure are included in the control system block

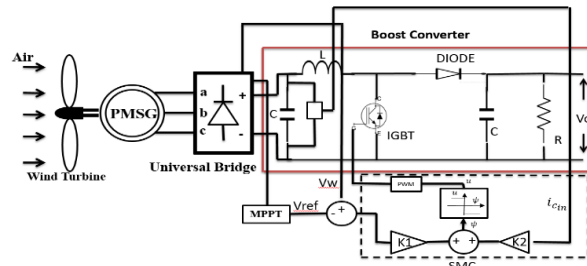diagram (Figure 5). The variable u is created by means of a comparator that has a zero centre.
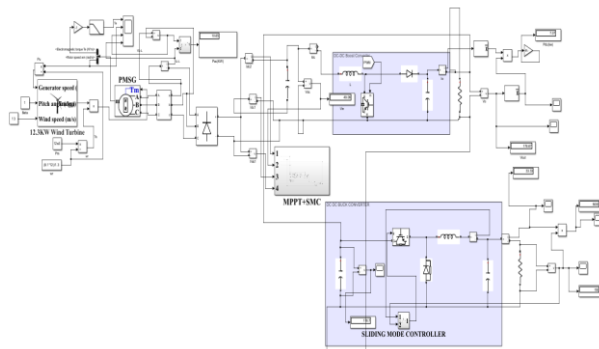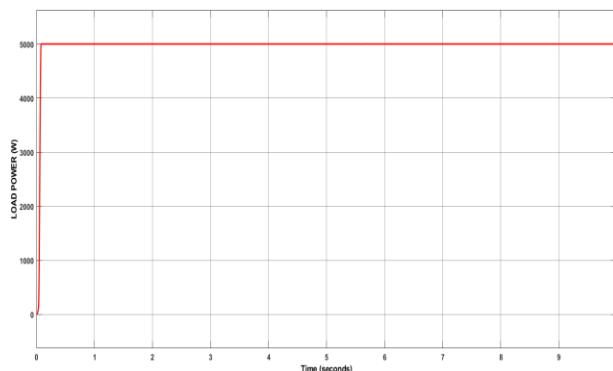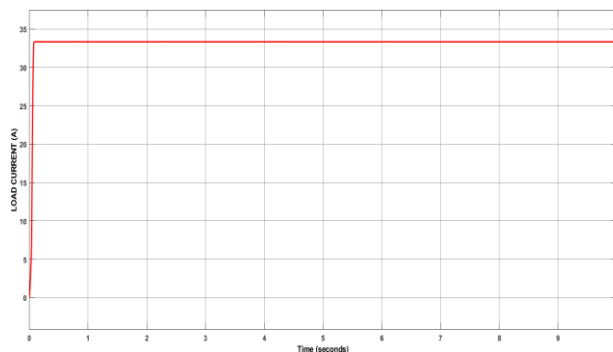

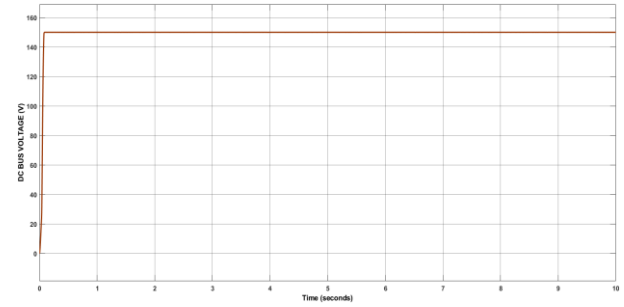**Fig. 5. Block diagram of SMC with P & O MPPT.**

Fig. 6. Wind turbine MATLAB model with SMC.

(a)

(b)

(c)

Fig. 7 (a) Wind turbine power for 5KW load, (b) wind current for 5KW load and (c) DC BUS voltage.

3.2 SMC Methodology for Diesel Generator

Sliding mode control (SMC) systems are a method for building systems that can withstand changes in parameters and external load disruptions. A high-speed switching control rule is used to carry out the strategy. It makes the path of the module follow a predefined course in the state variable space, also called a switching or sliding surface (a two-dimensional line). Reaching mode is defined as the control that is aimed toward the switching surface before the system actually reaches it. When a system is in sliding mode, its response is impervious to external perturbations and changes in specific parameters [18–21]. Nonlinear systems have been studied via the lens of the variable structure system (VSS) hypothesis. Its primary characteristic is that the error can be driven to a switching surface to initiate sliding mode. Sliding mode controllers (VSCs) are another name for variable structure controllers. Essentially, VSC is made up of several discrete continuous functions that connect the plant's status to a control surface represented by equation,

$$x(t) = Ax(t) + Bu(t) \qquad (22)$$

Which can be stated as

$$x(t) = f(x, t, u) \qquad (23)$$

The function vector is represented by f, and x denotes the state vector, and the control input, which is supplied to the switch, is symbolized by u. If $S(x) = 0$ is the so-called sliding surface where the function vector is discontinuous in sliding mode, then

$$f(x, t, u) = \begin{cases} f^*(x, t, u) & if \ s > 0 \\ f(x, t, u) & if \ s < 0 \end{cases}$$

Finding a control input u that will cause state vector x to follow the intended trajectory x^* is the control challenge in sliding mode theory. Shape-wise, the sliding surface is

$$S(x) = x_n - x_n^* \qquad (24)$$

If the initial condition is not met, tracking is not possible in order to compel the sliding surface of the system. You can accomplish this by

$$S_s \leq -\eta|S| \qquad (25)$$

Where η depicts the positive constant and S_s is the switching surface which fixes the output trajectories and hits it in a finite amount of time [21].

4. SMC CONTROLLER MODELING

This is the condition that the controller is trying to give:

$$\lim_{t \to \infty} V_c(t) = V_r \qquad (26)$$

If V_r represents the output reference DC voltages and the controller's staging is independent of both abrupt disturbances and system parameters in step-up converters.

A sliding surface for sliding motion must be identified for the purpose to implement a sliding control. For this reason, the sliding surface described in equation (27) is adopted.

$$S(x) = k_1(x_1 - I_r) + k_2(x_2 - V_r) \qquad (27)$$

Where I_r and V_r are the fuel cell's reference current and voltage, and k_1 and k_2 are the sliding surfaces constants.

The sliding mode is present when

$$S(x) = S(x) = 0 \qquad (28)$$

Two components make up the general control structure u and u_n, u_{eq} the equivalent control component.

$$u = u_n + u_{eq} \qquad (29)$$

The equivalent control is obtained using

$$u_{eq} = -\left[\frac{\partial S}{\partial x} B(x)\right]^{-1} \left(\frac{\partial S}{\partial x} Ax\right) \qquad (30)$$

Equation (27) can be differentiated with regard to x; we may obtain the values of A, B, and S(x) in this way S(x) as

$$\frac{\partial S}{\partial x} = [k_1 \ k_2] \qquad (31)$$

After solving we get

$$\left(\frac{\partial S}{\partial x} B(x)\right)^{-1} = \frac{LC}{[(k_1 C x_2 - k_2 L x_1)]} \qquad (32)$$

And,

$$\frac{\partial S}{\partial x} A(x) = \left[\frac{-k_1 x_2 RC + k_2 L(k_1 R - x_2 C)}{RLC}\right] \qquad (33)$$

Put Equations (17) (18) in (15) we get u_{eq} as

$$u_{eq} = \left[\frac{-k_1 x_2 RC + k_2 L(k_1 R - x_2 C)}{k_1 x_2 RC - k_2 x_1 RL}\right] \qquad (34)$$

Similarly,

$$u_n = k_3 sign(S(x)) \qquad (35)$$

When S is set from (27) to (28), the resulting controlling signal is

$$u = \left[\frac{-k_1 x_2 RC + k_2 L(k_1 R - x_2 C)}{k_1 x_2 RC - k_2 x_1 RL}\right] + k_3 sign(S(x)) \qquad (36)$$

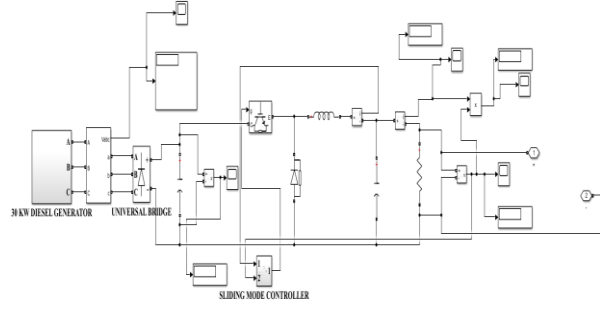The combined MATLAB/Simulink Module of SM Controller with diesel generator and buck converter is depicted in Figure 8.
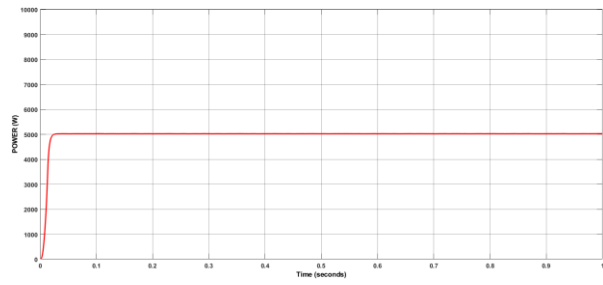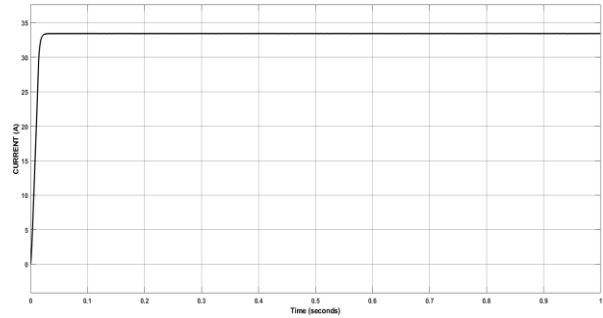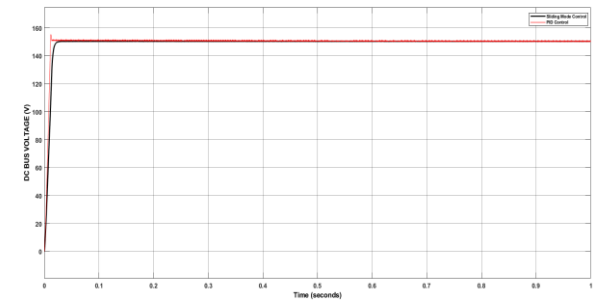

Fig. 8. Diesel generator model on MATLAB/ Simulink with buck converter.

(a)

(b)

(c)

Fig. 9. Diesel generators output results (a) current of generator, (b) power of generator, (c) output DC bus voltage with SMC and PI control..

5. MATLAB/SIMULATION RESULT

MATLAB/ Simulink is employed to evaluate the system's performance and model the overall system. As

seen in Figure 10, the primary energy sources are wind energy and diesel generator, with storage systems consisting of a battery and super capacitor. The SMC enables the DC grid voltage to revive again immediately and to maintain the DC grid voltage at 150V. The wind module is of total 12.3KW in combination with diesel generator of 30KW energy source. The pulsating loads attached with the microgrid at 1sec 5KW load is attached, the current of the DC grid is increased to 33.33A.the result of output DC grid voltage and current is shown in Figure 11. On 2sec another 10KW load is added on now the total load on the system is 15KW the current of the DC grid is increased 100A. On 3sec time another pulsating load of 15KW is attached on the load now the total load on the system 30KW now the current of the system is increased to 200A.the total generation of energy source is 42.3 KW and the combined load on the module is 40KW.the SMC is the robust control which maintain the DC grid voltage to a certain level of 150V. In order to maintain the grid voltage, the battery and super capacitor's current, voltage, and SOC% fluctuate together. Figures 12, 13, display the battery and super capacitor's output waveform.
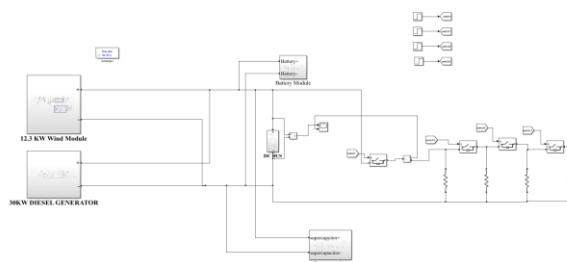

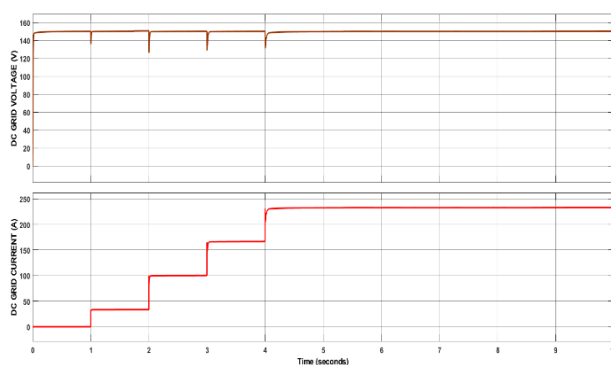**Fig. 10. Matlab/Simulink model of combined wind and diesel generator with pulsating loads**.

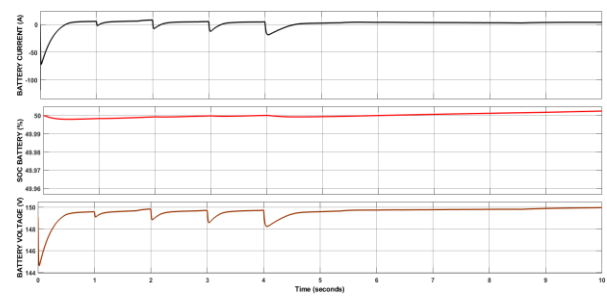**Fig. 11. DC grid voltage and current and different loads.**

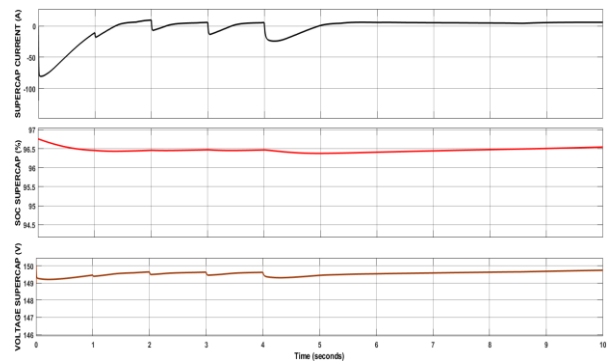**Fig. 12. battery current, voltage and % SOC of battery.**

Fig. 13. Super capacitor current, voltage and SOC.

6.   CONCLUSION

This study shows the effectiveness of sliding mode control in ensuring robust and reliable operation of DC microgrid with a variety of energy storage devices and RES, particularly in the presence of pulsating loads. In the conclusion, SMC for a DC microgrid powered by diesel generator, wind turbine, with energy storage system on pulsating loads is discussed. We have demonstrated through rigorous simulations and analysis that, as compared to typical PI control approaches, sliding mode control delivers higher performance in monitoring intended set points, minimizing disturbances, and enhancing system stability. The knowledge gathered from this study not only advances microgrid control strategies but also has practical applications that could lead to more robust and sustainable energy systems. Moving forward, further investigations could focus on refining control algorithms, integrating advanced predictive techniques, and validating experimental results to accelerate the transition towards smarter and more efficient microgrid solutions in the renewable energy landscape.

7.   FUTURE SCOPE

In future the combination of solar PV, fuel cell, wind generator and diesel generator is used and controlled by sliding mode control to check the voltage regulation. System stability and robustness of the controller to maintain the grid voltage in different loading conditions (under load, full load and over load) as well as the input change to RES (irradiance change with time to solar

module, air wind speed changes with time to wind module and hydrogen rate change to fuel cell module) the controller behavior to maintain the grid voltage and different comparative study with different controllers like droop, adaptive droop, *etc*.

REFERENCES

[1] Jacob H. and X. Wang. 2015. Sliding mode control of a permanent magnet synchronous generator for variable speed wind energy conversion systems. *Systems Science & Control Engineering* 3(1): 453-459.

[2] Guerrero J.M., Chandorkar M., Lee T.L., and Loh, P.C., 2013. Advanced control architectures for intelligent microgrids—Part II: Power quality, energy storage, and AC/DC microgrids. *IEEE Transactions on Industrial Electronics* 60(4), 1263-1270.

[3] Dragicevic T., Lu X., and Vasquez J.C., 2016. DC microgrids—Part I: A review of control strategies and stabilization techniques. *IEEE Transactions on Power Electronics* 31(7), 4876-4889.

[4] Mousavi Y., Geraint Bevan I.B., Kucukdemiral, A.F., Sliding mode control of wind energy conversion systems: Trends and applications, *Renewable and Sustainable Energy Reviews*.

[5] Xiao J. and P. Wang. 2013. Multiple modes control of household DC microgrid with integration of various renewable energy sources. In *Industrial Electronics Society, IECON 2013 - 39th Annual Conference of the IEEE*, 2013, pp. 1773-1778.

[6] Lirong Z., Yi W., Heming L., and Pin S., 2012. Hierarchical coordinated control of DC microgrid with wind turbines. In *IECON 2012 - 38th Annual Conference on IEEE Industrial Electronics Society*, 2012, pp. 3547-3552.

[7] Esram T. and P.L. Chapman. 2007. Comparison of photovoltaic array maximum power point tracking techniques. *IEEE Transactions on Energy Conversion* 22(2), 439-449.

[8] Hau E., 2006. Wind Turbines—Fundamentals, Technologies, Application and Economics, 2nd ed.; Springer: Berlin/Heidelberg, Germany.

[9] Heier S., 2014. Grid Integration of Wind Energy: Onshore and Offshore Conversion Systems; John Wiley & Sons: Hoboken, NJ, USA.

[10] Abdullah M.A., Yatim A.H.M., and Tan C.W.A., 2011. Study of maximum power point tracking algorithms for wind energy system. In *Proceedings of the IEEE First Conference on Clean Energy and Techonology (CET)*, Kuala Lumpur, Malaysia, 27–29 June 2011; pp. 321–326.

[11] Abdullah M.A., Yatim A.H.M., Tan C.W., Saidur R., 2012. A review of maximum power point tracking algorithms for wind energy systems. *Renewable and Sustainable Energy Reviews* 16, 3220–3227.

[12] Sadick A., 2023. Maximum Power Point Tracking Simulation for Photovoltaic Systems Using Perturb and Observe Algorithm', Solar Radiation - Enabling Technologies, Recent Innovations, and Advancements for Energy Transition [Working Title]. IntechOpen, May 11, 2023. doi: 10.5772/intechopen.111632.

[13] Senjyu T., Nakaji T., Uezato K., and Funabashi T., 2005. A hybrid power system using alternative energy facilities on an isolated island. *IEEE Transactions on Energy Conversion* 20(2): 406–414.

[14] Rakopoulos, Constantine D., Giakoumis, and Evangelos G., 2009. Diesel Engine Transient Operation- Principles of Operation and Simulation Analysis, Springer, 2009.

[15] Stavrakakis G.S. and G.N. Kariniotakis. 1995. A general simulation algorithm for the accurate assessment of isolated diesel- wind turbines systems interaction. *IEEE Transactions on Energy Conversion* 10(3): 577–583.

[16] Sharaf A.M. and E.S. Abdin. 1989. A digital simulation model for wind-diesel conversion scheme. 26-28 Mar 1989, pp. 160–166.

[17] Wamkeue R., Baetscher F., and Kamwa I., 2008. Hybrid state model-based time-domain identification of synchronous machine parameters from saturated load rejection test records. *IEEE Transactions on Energy Conversion*, vol. 23, no. 1, pp. 68–77, 2008.

[18] Wang Z., Li S. and Li Q., 2020. Continuous Nonsingular Terminal Sliding Mode Control of DC–DC Boost Converters Subject to Time-Varying Disturbances. In *IEEE Transactions on Circuits and Systems II: Express Briefs*, vol. 67, no. 11, pp. 2552-2556, Nov. 2020

[19] Petrone G. and C. Ramos-Paja. 2011. Modeling of photovoltaic fields in mismatched conditions for energy yield evaluations. *Electric Power Systems Research* 81, no. 4, pp. 1003–1013, 2011.

[20] Bianconi E., Calvente J., Giral R., Mamarelis E., Petrone G., Ramos-Paja C.A., Spagnuolo G., and Vitelli M., 2013. A fast current based MPPT technique employing sliding mode control. *IEEE Transactions on Industrial Electronics* 60, no. 3, pp. 1168–1178, 2013.

[21] Joshi K.R. and H.V Kannad. 2015. Design of Sliding Mode Control for BUCK Converter, pp. 4001-4008.